Analysis of the shell effect of fission fragments in the quasi-fission process

Hokuto Maekawa[1,*], *Shota* Amano[1], *Shinya* Takagi[1], and *Yoshihiro* Aritomo[1]

[1]Graduate School of Science and Engineering, Kindai University, Higashi-Osaka, Osaka, Japan

Abstract. The process in superheavy element synthesis in which two nuclei collide and fission before forming a compound nucleus is called quasi-fission. The dynamical model used in our calculations is highly reproducible in calculating the total kinetic energy (TKE) of actinide fission. However, there is a problem in the reproducibility of TKE of quasi-fission in the current calculations using the dynamical model. Our calculations show that the TKE of mass asymmetry is lower than the experimental data. The reason for this is that the shell effect of fission fragments is not considered. In this study, we attempted to reproduce mass-asymmetric quasi-fission with shell effects by using a dynamical model. The objective is to analyze the calculation results and follow the time evolution of the shape of the nucleus to deepen our understanding of the dynamics of quasi-fission.

1 Introduction

The mass asymmetric quasi-fission events is experimentally observed to be dominated by the mass number 207 u−209 u[1, 2]. These observations suggest that closed spherical shells contribute to the production of mass asymmetric quasi-fission. The shell effect of the octupole deformation at Z=52,56 explains the experimentally observed asymmetric fission[3].

2 Model

We adopt the dynamical model that can trace evolution of the heavy nuclear system. We perform a trajectory calculation on potential energy surfaces.

2.1 Potential energy

The potential energy is described using two different potential energies to calculate the fusion-fission process. The potential energy between two nuclei at infinity that crosses the Coulomb barrier and comes into contact with each other is called the diabatic potential. $f(t)$ is a function of time, $V_{diaba}(q)$ is the diabatic potential energy $V_{ADIABA}(q, \ell, T)$ is the adiabatic potential energy and t is reaction time and τ is the relaxation time. $g(z)$ is the distance between nuclei and ζ_x is the relaxation distance.

$$V = f(t)V_{diaba}(q) + (1 - f(t))V_{ADIABA}(q, \ell, T) \quad (1)$$

$$f(t) = \frac{1}{\exp\left(-\frac{t}{\tau_i}\right)} \quad (2)$$

$$V_{ADIABA} = g(z)V_{adiaba}(q) + (1 - g(z))V_{diaba}(q, \ell, T) \quad (3)$$

$$g(z) = \frac{1}{\left\{1 + \exp\left(-\frac{z}{\zeta_x}\right)\right\}^2} \quad (4)$$

*e-mail: 22333404r@kindai.ac.jp

2.2 Two Center Shell Model

The shape of the nucleus is shown in figure1. The distance z between the centers of the nuclei and the mass asymmetry degree α deformation degree δ are expressed by the following equations[4].

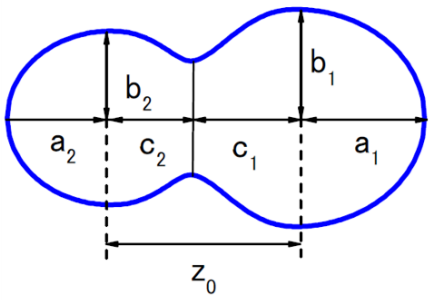

Figure 1. Shape of nuclei by the two-center-shell model

$$z_0 = |c_1| + |c_2| \quad (5)$$

$$\delta = \frac{3(a - b)}{2a - b} \quad (6)$$

$$\alpha = \frac{A_1 - A_2}{A_1 + A_2} \quad (7)$$

$$B = \frac{3 + \delta}{3 - 2\delta} \quad (8)$$

$$z = \frac{z_0}{R_{CN}B} \quad (9)$$

2.3 Multidimensional Langevin equation

Since relative motion must be taken into account in the fusion process where two nuclei approach each other, the multidimensional Langevin equation is as follows[5, 6]. q_i is the variable for the shape of the nucleus and p_i is

the conjugate momentum of q_i. m_{ij} and γ_{ij} are the mass of inertia and friction coefficient, respectively, which depend on the geometry of the nucleus. These are also called transport coefficients. $R_j(t)$ is a normalized random variable that follows a Gaussian distribution, and g_{ij} is the random force.

$$\frac{\mathrm{d}q_i}{\mathrm{d}t} = \left(m^{-1}\right)_{ij} p_j \tag{10}$$

$$\frac{\mathrm{d}p_i}{\mathrm{d}t} = -\frac{\partial V}{\partial q_i} - \frac{1}{2}\frac{\partial}{\partial q_i}\left(m^{-1}\right)_{jk} p_j p_k - \gamma_{ij}\left(m^{-1}\right)_{jk} p_k + g_{ij} R_j(t) \tag{11}$$

$$\frac{\mathrm{d}\theta}{\mathrm{d}t} = \frac{\ell}{\mu_R R^2} \tag{12}$$

$$\frac{\mathrm{d}\varphi_1}{\mathrm{d}t} = \frac{L_1}{\Im_1} \tag{13}$$

$$\frac{\mathrm{d}\varphi_2}{\mathrm{d}t} = \frac{L_2}{\Im_2} \tag{14}$$

$$\frac{\mathrm{d}\ell}{\mathrm{d}t} = -\frac{\partial V}{\partial \theta} - \gamma_{tan}\left(\frac{\ell}{\mu_R R^2} - \frac{L_1}{\Im_1}a_1 - \frac{L_2}{\Im_2}a_2\right)R + R g_{tan} R_{tan}(t) \tag{15}$$

$$\frac{\mathrm{d}L_1}{\mathrm{d}t} = -\frac{\partial V}{\partial \varphi_1} + \gamma_{tan}\left(\frac{\ell}{\mu_R R^2} - \frac{L_1}{\Im_1}a_1 - \frac{L_2}{\Im_2}a_2\right)a_1 + a_1 g_{tan} R_{tan}(t) \tag{16}$$

$$\frac{\mathrm{d}L_2}{\mathrm{d}t} = -\frac{\partial V}{\partial \varphi_2} + \gamma_{tan}\left(\frac{\ell}{\mu_R R^2} - \frac{L_1}{\Im_1}a_1 - \frac{L_2}{\Im_2}a_2\right)a_2 + a_2 g_{tan} R_{tan}(t) \tag{17}$$

3 Resuts and Discussion

The effect of shell structure with the present framework is described below. Figure2 shows the mass distribution for with or without shell correction energy, and with or without diabatic potential in the reaction system of ^{48}Ca+^{238}U.

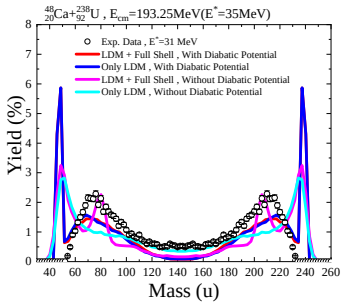

Figure 2. Mass distribution of ^{48}Ca+^{238}U system at excitation energies 35 MeV calculated by dynamical model. The red line is Calculated with shell correction energy and diabatic potential. The blue line is Calculated without shell correction energy and with diabatic potential. The magenta line is Calculated with shell correction energy and without diabatic potential. The cyan line is Calculated without shell correction energy and diabatic potential. Black circles are the experimental value at excitation energies 31 MeV[7].

The 48 u and 238 u peaks in the mass distribution are elastic scattering events. Comparing the red and blue lines, it can be seen that there is no difference in the mass distribution with and without the shell correction energy when the diabatic potential is introduced. Both the red and blue lines have a peak at 220 u. On the other hand, comparing the magenta and cyan lines, there is a difference in the mass distribution with and without the shell correction energy when the diabatic potential is removed. The magenta line has sharp peak at 210 u. The cyan lines have no peaks, except for elastic scattering events. The red, blue and magenta line peaks are expected to be due to the ^{208}Pb shell effect. However, the peaks of 210 u and 220 u are a little bit different. We discuss this difference.

It is known that fission fragments due to the shell effect of ^{208}Pb are generally spherical in shape. The mass asymmetric α and the deformation of fragments δ distribution of fission fragments in the results of Fig.2 is shown in Fig.3.

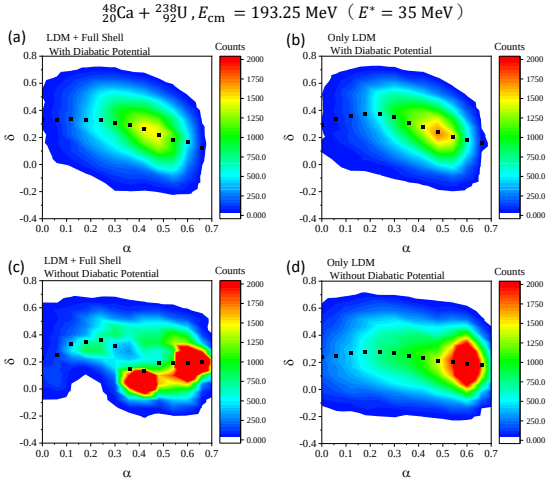

Figure 3. $\alpha - \delta$ distribution panel (a): Calculated with shell correction energy and diabatic potential panel (b): Calculated without shell correction energy and with diabatic potential panel (c): Calculated with shell correction energy and without diabatic potential panel (d): Calculated without shell correction energy and diabatic potential The black dots are the averages of δ with respect to α

Panels (a) , (b) and (d) do not differ significantly in the degree of deformation. Panel (c) shows a small degree of deformation at $\alpha = 0.45$. Panel (c) that the spherical shell effect due to ^{208}Pb is applied. The presence or absence of an adiabatic potential in the calculation of the potential with the introduction of shell correction energy determines whether or not the shell effect is received. Figure4 shows sample trajectories under the panels (a) and (c) calculation conditions.

In the $z - \delta$ plane, the black line is strongly affected by the potential of panel (a). Since the diabatic potential is treated as a two-body nucleus, where the two nuclei overlap, the potential energy increases rapidly due to high density. The black line is inhibited by the potential energy surge. On the other hand the gray line is strongly affected by the potential of panel (b). Thus, the gray line can easily proceed to the interior. We compare these trajectories in

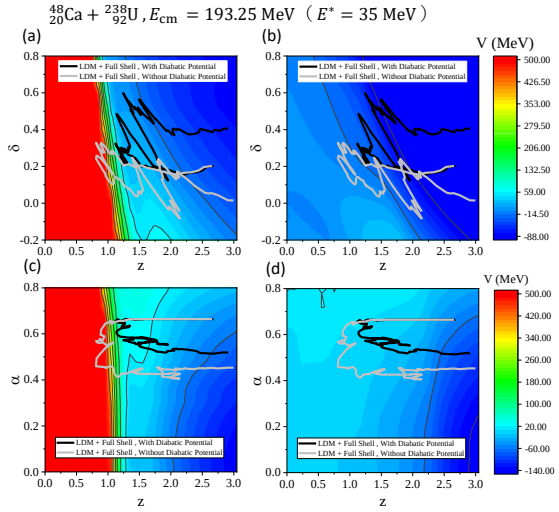

Figure 4. Sample trajectories are calculated by dynamical model. Gray trajectory is calculated with shell correction energy and diabatic potential. Black trajectory is calculated with shell correction energy and without diabatic potential. panel (a): The potential energy surface of the diabatic potential on the $z-\delta$ plane for ^{48}Ca+^{238}U system panel (b): The potential energy surface of the adiabatic potential on the $z-\delta$ plane for ^{286}Cn panel (c): The potential energy surface of the diabatic potential on the $z-\alpha$ plane for ^{48}Ca+^{238}U system panel (d): The potential energy surface of the adiabatic potential on the $z-\alpha$ plane for ^{286}Cn

the $z-\alpha$ plane. Panel (c) shows that the black line is impeded by a sharp increase in potential energy, but the mass asymmetry is smaller.

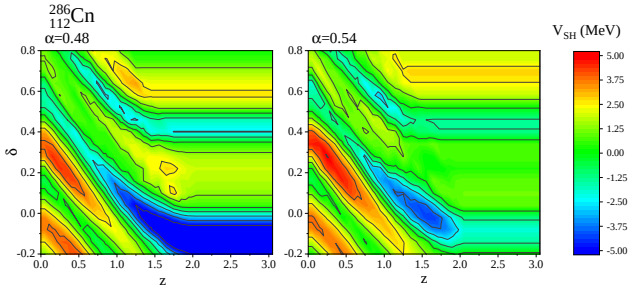

Figure 5. Color map of shell correction energy on the $z-\delta$ plane for ^{286}Cn. The mass asymmetric α is 0.48 (left). The mass asymmetric α is 0.54 (right).

Figure5 shows the shell correction at each α. Even at $\alpha = 0.45$ and $\alpha = 0.54$, there are regions where the shell correction energy is small due to the ^{208}Pb shell effect. Some differences in mass asymmetry appear depending on the presence or absence of diabatic potentials. These differences, however, have little effect on whether or not the shell effect is received. The key to receiving the shell effect is the degree of deformation. In the process of two nuclei colliding and transferring nucleons, it is better to keep the deformation degree of nuclei small to receive the ^{208}Pb shell effect.

4 Summary

This study describes the differences in mass fractions and TKE between diabatic potential energy dominated and adiabatic potential energy dominated fission fragments in the quasi-fission process. It was found that the shape just before fission must be compact in order to produce fission fragments that are subject to the ^{208}Pb induced spherical shell effect.

References

[1] E. M. Kozulin, G. N. Knyazheva, et al., Phys. Lett. B **686**, 227 (2010)
[2] A. Wakhle, C. Simenel, D. J. Hinde, et al., Phys. Rev. Lett. **113**, 182502 (2014)
[3] Guillaume Scamps, Cédric Sminel Nature **564**, (2018)
[4] Joachim Maruhn and Walter Greiner, Z. Physik **251**, 431-457 (1972)
[5] V. Zagrebaev and W. Greiner, J. Phys. G **31**, 825 (2005)
[6] A. V. Karpov and V. V. Saiko, Phys. Rev. C **96**, 024618 (2017)
[7] K. Nishio, S. Mitsuoka, et al., Phys. Rev. C **86**, 034608 (2012)